IET Generation, Transmission & Distribution

Research Article

IET Journals
The Institution of Engineering and Technology

Design of LCC HVDC wide-area emergency power support control based on adaptive dynamic surface control

ISSN 1751-8687
Received on 14th September 2016
Revised 26th March 2017
Accepted on 25th April 2017
E-First on 17th July 2017
doi: 10.1049/iet-gtd.2016.1472
www.ietdl.org

Chongru Liu[1] ✉, *Yunhao Zhao*[2], *Gengyin Li*[1], *Udaya D. Annakkage*[3]

[1]*State Key Laboratory for Alternate Electrical Power System with Renewable Energy Sources, North China Electric Power University, 2# Beinong road, Changping district, Beijing, People's Republic of China*

[2]*State Nuclear Electric Power Planning Design & Research Institute CO., LTD, 6# Dijin road, Haidian District, Beijing, People's Republic of China*

[3]*Department of Electrical and Computer Engineering, University of Manitoba, R3T 2N2, Winnipeg, Canada*

✉ *E-mail: chongru.Liu@ncepu.edu.cn*

Abstract: In AC–DC parallel systems, line-commutated-converter (LCC)-based high-voltage direct-current (HVDC) emergency control strategy can improve the stability of the power system. This study proposes an LCC HVDC emergency control strategy that utilises the global information measured by wide-area measurement systems. The design of the proposed LCC HVDC emergency control strategy takes advantage of dynamic surface control and adaptive control. The Lyapunov stability analysis is used to prove that the AC–DC parallel system is uniformly ultimately bounded in the presence of the uncertainties. A two-area four-generator AC–DC parallel system is developed in PSCAD/EMTDC to verify the effectiveness and correctness of the proposed strategy. Simulation results show that the proposed LCC HVDC emergency control strategy can improve the stability of an AC–DC parallel system and is robust. Its superiority is demonstrated by comparing the proposed method with controllers designed using backstepping technique and pole placement technique.

1 Introduction

The line-commutated-converter (LCC)-based high-voltage direct-current (HVDC) technology has been widely adopted in the world because of its advantages in long-distance large-scale transmission [1, 2]. Especially in China, in order to address the problem that power centre and load centre are distributed unequally and regional grids are needed to be interconnected, LCC HVDC transmission system has played an important role in transmitting the power from the power centre to load centre and interconnecting regional grids. As a result, AC–DC parallel power systems become more and more common. For example, China Southern Power Gird is a parallel AC–DC power grid [3]. In these parallel power systems, the ability of an LCC HVDC system to rapidly change its power can be used to design effective and economical LCC HVDC emergency power control strategies to improve the transient stability of the AC–DC parallel power systems [4].

The traditional LCC HVDC emergency control utilises linear control system methods to design the controllers. The active power of AC transmission line operating in parallel with DC system is typically used as the input signal of the emergency control strategy [5, 6]. Linear control system design does not take into account any parameter uncertainties.

The developments of wide-area measurement systems (WAMSs) [7, 8] and robust non-linear schemes [9–12] have brought new opportunities to design the LCC HVDC emergency power control. A non-linear robust control law, such as feedback linearisation method, sliding mode control and backstepping control technique, has been used to design the LCC HVDC emergency power control strategy based on the global signals of the AC–DC parallel system measured by WAMS. These schemes are generally referred to as LCC HVDC wide-area emergency power control [13–15]. However, the feedback linearisation method needs the accurate model of the AC–DC parallel system and cannot deal with the uncertain modelling error of the system or external disturbance sufficiently. The LCC HVDC wide-area emergency power control strategy based on sliding mode control is discontinuous and unsmooth. Discontinuous control laws are known to display chattering phenomena and excite high frequency unmodeled dynamics [16]. The LCC HVDC wide-area emergency power control strategy based on backstepping technique is continuous. However, there is a high computational burden in conventional backstepping technique, and thus the design process of is complicated and the control rule is complex. The dynamic surface control (DSC) has been proposed to solve this problem by introducing a first-order filter. As a result, the control rule is continuous. In addition, the control rule and the design process are simpler than backstepping technique [17, 18]. However, the conventional DSC is not immune to parameter uncertainties, unknown modelling error and external disturbances which are common in dynamic systems.

In order to make the DSC more applicable for dynamical systems, DSC is used with adaptive control schemes together to make the control strategy. A constraints transformation-based robust adaptive DSC method is used to make a tracking controller capable of achieving output tracking objective for a class of non-linear systems with parameter uncertainties and output constraints in [19]. A DSC-based adaptive fuzzy method is used to design a good performance of position tracking control for induction motors used in electric vehicle drive system in [20], and the DSC and adaptive fuzzy control are used together to design a control strategy for APF to improve the system response speed in [21]. What's more, the DSC and adaptive control schemes have been used in flexible spacecraft, transport aircraft with continuous heavy cargo airdrop, unmanned aerial vehicle, permanent magnet synchronous motor, robot manipulators, MEMS gyroscope, vehicle active suspension systems and other equipments successfully [22–28], but the DSC and adaptive control are not used to design an LCC HVDC wide-area emergency controller with good performance in AC–DC parallel power systems.

To promote the application of DSC and adaptive control schemes for AC–DC parallel power systems, this paper proposes an LCC HVDC wide-area emergency controller based on DSC and adaptive control schemes. The proposed control strategy not only can take the advantage of DSC that the control rule is continuous and simpler than the control strategy based on the backstepping technique, but also can deal with the parameter uncertainties, unknown modelling error and external disturbances.

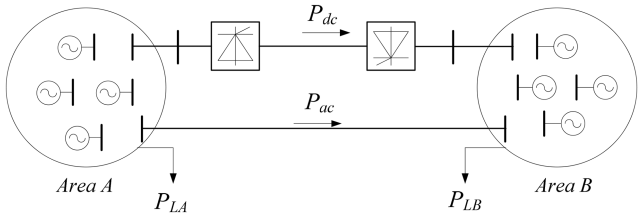

Fig. 1 *Sketch of the AC/DC interconnected two-area power system*

The paper is organised as follows: Section 2 analyses the mathematical model of AC–DC parallel system based on centre of inertia (COI) using WAMS signals, Section 3 designs the LCC HVDC wide-area emergency control strategy based on the DSC strategy and adaptive control schemes, Section 4 demonstrates the stability analysis of the proposed strategy, Section 5 tests the control strategy and design method in a two-area four-generator AC–DC parallel power system. The general conclusions are presented in Section 6.

2 WAMS-based mathematical model of AC–DC parallel power system

With the rapid development of the HVDC technology, the AC–DC parallel transmission lines connecting two regional power grids are becoming more and more universal. An equivalent structure of an AC–DC parallel power system shown in Fig. 1 is used in this paper to demonstrate the proposed methodology. The AC system is divided into two areas (Areas A and B) by the AC and DC parallel transmission lines, Areas A and B are the sending area and receiving area, respectively. Suppose the angular speed of each generator and the active power of LCC HVDC system and AC line linking Areas A and B are accessible with phasor measurement units (PMUs)s equipped in the system.

According to COI-based equivalent method, the angular speed of COI-based equivalent generator of Areas A and B, $\omega_{\mathrm{COI},A}$ and $\omega_{\mathrm{COI},B}$, as shown in (1) [29]:

$$\begin{cases} \omega_{\mathrm{COI},A} = \sum_{i \in A}^{n_A} H_i \omega_i / H_{T,A} \\ \omega_{\mathrm{COI},B} = \sum_{i \in B}^{n_B} H_i \omega_i / H_{T,A} \end{cases} \tag{1}$$

where ω_i is the angular speed of the ith generator and is in per unit; H_i is the inertia constants of the ith generator and its unit is s; $H_{T,A}$ and $H_{T,B}$ are the COI-based equivalent inertia constant of Areas A and B, respectively, and they can be computed as shown in the following equation:

$$\begin{cases} H_{T,A} = \sum_{i \in A}^{n_A} H_i \\ H_{T,B} = \sum_{i \in A}^{n_B} H_i \end{cases} \tag{2}$$

The swing equations of COI-based equivalent generators of Areas A and B as shown in the following equation:

$$\begin{cases} 2H_{T,A}\dot{\omega}_{\mathrm{COI},A} = \sum_{i \in A}(P_{\mathrm{mi}} - P_{\mathrm{ei}}) - \sum_{i \in A} D_i(\omega_i - 1) \\ 2H_{T,B}\dot{\omega}_{\mathrm{COI},B} = \sum_{i \in B}(P_{\mathrm{mi}} - P_{\mathrm{ei}}) - \sum_{i \in B} D_i(\omega_i - 1) \end{cases} \tag{3}$$

where the P_{mi}, P_{ei} and D_i are the prime mover input power, the active power output and the damping coefficient of the ith generator, respectively. Only $H_{T,A}$ and $H_{T,B}$ are actual value variables and the unit is seconds. The other variables are all in per unit.

The power flow equations of the Areas A and B based on the principle of conservation of energy as shown in the following equation:

$$\begin{cases} \sum_{i \in A} P_{\mathrm{ei}} = P_{\mathrm{L}A} + P_{\mathrm{dc}} + P_{\mathrm{ac}} \\ \sum_{i \in B} P_{\mathrm{ei}} = P_{\mathrm{L}B} - P_{\mathrm{dc}} - P_{\mathrm{ac}} \end{cases} \tag{4}$$

where $P_{\mathrm{L}A}$, $P_{\mathrm{L}B}$ are the sum of load and network power loss of Areas A and B, respectively, P_{dc} and P_{ac} are the active power of LCC HVDC system and interconnected AC line, respectively.

The LCC HVDC system is modelled as a first-order inertial object in studying the stability of AC–DC parallel power system [30] and the model as shown in the following equation:

$$\dot{P}_{\mathrm{dc}} = \frac{1}{T_{\mathrm{d}}}(-P_{\mathrm{dc}} + P_{\mathrm{dcREF}} + u_{\mathrm{dc}}) \tag{5}$$

where P_{dcREF} is the reference setting of the LCC HVDC system; T_{d} is the equivalent time constant of the DC system ($T_{\mathrm{d}} = 0.2$ s in this paper); and u_{dc} is the emergency power control signal of the LCC HVDC system.

By using the equivalent velocity of the centre area B as the reference and incorporating the modelling error and external disturbance, the COI-based mathematical model of the AC–DC parallel system can be expressed

$$\begin{cases} \dot{\omega}_{\mathrm{COI},A} - \dot{\omega}_{\mathrm{COI},B} = \dfrac{\sum_{i \in A}(P_{\mathrm{mi}} - P_{\mathrm{ei}})}{2H_{T,A}} - \dfrac{\sum_{i \in B}(P_{\mathrm{mi}} - P_{\mathrm{ei}})}{2H_{T,B}} \\ \quad + \underset{\mathrm{COI}}{\tilde{D}}(\omega_{\mathrm{COI},A} - \omega_{\mathrm{COI},B}) + e_{\mathrm{R}} + e_{\mathrm{G}} \\ \dot{P}_{\mathrm{dc}} = \dfrac{1}{T_{\mathrm{d}}}(-P_{\mathrm{dc}} + P_{\mathrm{dcREF}} + u_{\mathrm{dc}}) + e_{\mathrm{D}} \end{cases} \tag{6}$$

where

$$\underset{\mathrm{COI}}{\tilde{D}}(\omega_{\mathrm{COI},A} - \omega_{\mathrm{COI},B}) + e_{\mathrm{R}} = -\frac{1}{2H_{T,A}}\sum_{i \in A} D_i(\omega_i - 1) + \frac{1}{2H_{T,B}}\sum_{i \in B} D_i(\omega_i - 1)$$

$\underset{\mathrm{COI}}{\tilde{D}}$ is the COI-based equivalent damping factor of the AC–DC parallel system; e_{R} is the modelling error of this equivalent damping factor; e_{G} is the modelling error and external disturbance of COI-based equivalent model; e_{D} is the modelling error and external disturbance of the LCC HVDC system. All of these four parameters are uncertain parameters as they cannot be measured and calculated.

3 Design of control strategy and stability analysis

3.1 State space of AC–DC parallel system

The state space of AC–DC parallel system is needed first to design the LCC HVDC emergency control strategy. It is desired to eliminate the difference between the COI-based equivalent angular speed of Areas A and B. Therefore, the control target of LCC HVDC emergency control is

$$\omega_{\mathrm{COI},A} - \omega_{\mathrm{COI},B} = 0 \tag{7}$$

Let us define two state variables x_1 and x_2 as the speed difference and the derivative of speed difference and an output y as shown in the following equation:

$$\begin{aligned} x_1 &= \omega_{\mathrm{COI},A} - \omega_{\mathrm{COI},B} \\ x_2 &= \dot{\omega}_{\mathrm{COI},A} - \dot{\omega}_{\mathrm{COI},B} \\ y &= x_1 \end{aligned} \tag{8}$$

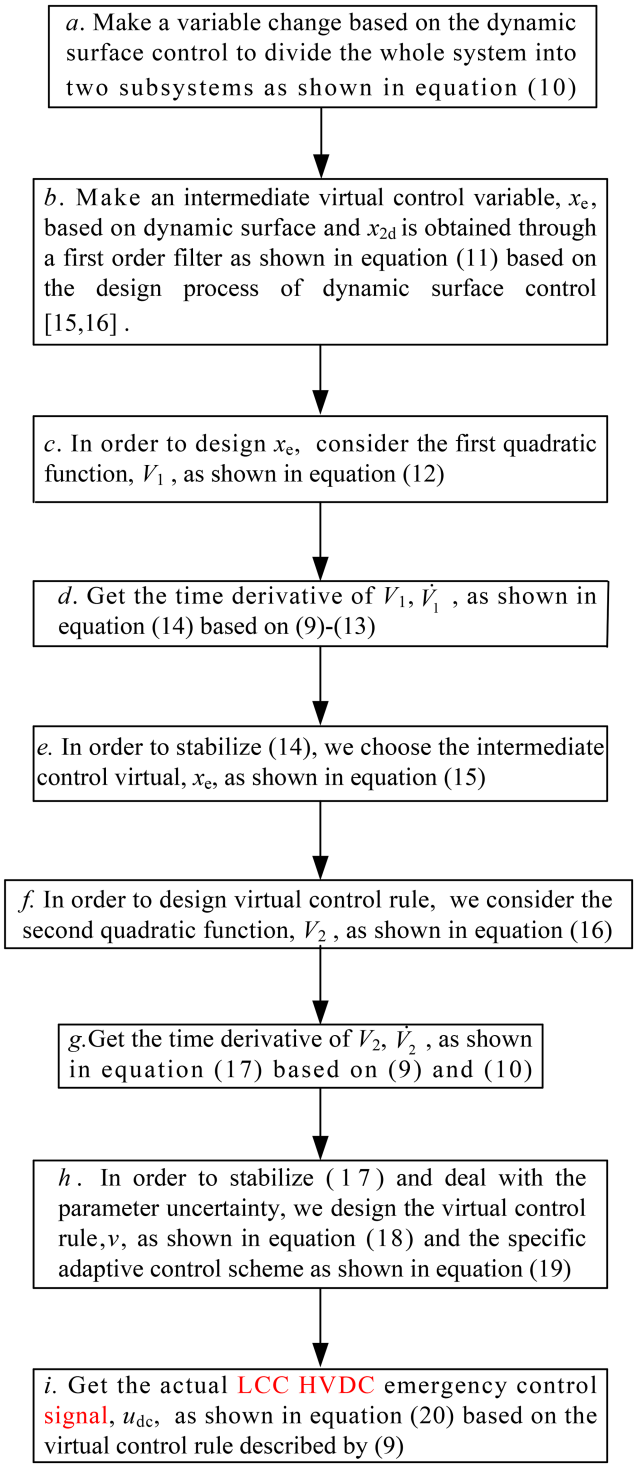

Fig. 2 *Design process flowchart of the control strategy*

In order to apply the DSC strategy and adaptive control scheme, the power system model described above needs to be presented in the standardised format for controller design. The standardisation of the state space of the AC–DC system as shown in the following equation:

$$\begin{cases} \dot{x}_1 = x_2 \\ \dot{x}_2 = v + \theta^* x_2 + \Delta(t) \end{cases} \tag{9}$$

where

$$v = \frac{\sum_{i\in A}\dot{P}_{mi} - \dot{P}_{LA} - \dot{P}_{ac}}{2H_{T,A}} - \frac{\sum_{i\in B}\dot{P}_{mi} - \dot{P}_{LB} + \dot{P}_{ac}}{2H_{T,B}} - \frac{(H_{T,B}+H_{T,A})}{2H_{T,A}H_{T,B}}\left[\frac{1}{T_d}(-P_{dc} + P_{dcREF} + u_{dc})\right],$$

$$\theta^* = \underset{COI}{\tilde{D}},$$

$$\Delta(t) = -\frac{(H_{T,B}+H_{T,A})}{2H_{T,A}H_{T,B}}e_D + \dot{e}_R + \dot{e}_G .$$

where v and u_{dc} are the virtual and actual control variables of the system, respectively; θ^* is the uncertain parameter used to represent the COI-based equivalent damping factor $\underset{COI}{\tilde{D}}$; $\Delta(t)$ is used to represent the uncertain integrated modelling error and integrated external disturbance, $\Delta(t)$ satisfies that $|\Delta(t)| \le \psi^*$ and $\psi^*$is a uncertain parameter.

3.2 Design of control strategy

The basic DSC method does not accommodate parameter uncertainties. In order to take the advantages of DSC and at the same time regulate the effect of uncertain parameters, in the proposed approach, we combine adaptive control based on certainty equivalence principle [19] and a variant of the σ-modification [24] which can deal with these parameter uncertainties with DSC. The design process flowchart is shown in Fig. 2 and the design process of the control strategy is shown below.

First, make a variable change based on the DSC to divide the whole system into two subsystems as there are two state variables in the state space of AC–DC parallel system [17, 18]

$$\begin{cases} S_1 := x_1 \\ S_2 := x_2 - x_{2d} \end{cases} \tag{10}$$

To make the LCC HVDC emergency control strategy combined the adaptive control with DSC, we make an intermediate virtual control variable, x_e, first.

x_{2d} is obtained through a first-order filter as shown in (11) based on the design process of DSC [17, 18] and by doing this the control strategy based on DSC is simpler than the control strategy based on backstepping control

$$\tau\dot{x}_{2d} + x_{2d} = x_e, \quad x_{2d}(0) = x_e(0) \tag{11}$$

where τ is a design time constant of the first-order filter.

To make the intermediate control virtual x_e, we consider the first quadratic function as shown in the following equation:

$$V_1 = \frac{1}{2}S_1^2 \tag{12}$$

In order to design the control strategy and stability analysis, we define the filtering error y_2 as shown in the following equation:

$$y_2 = x_{2d} - x_e \tag{13}$$

Considering (9)–(13), the time derivative of V_1 can be expressed as

$$\begin{aligned} \dot{V}_1 &= S_1\dot{S}_1 = S_1x_2 = S_1(S_2 + y_2 + x_e) \\ &\le S_1x_e + 2S_1^2 + \frac{1}{4}S_2^2 + \frac{1}{4}y_2^2 \end{aligned} \tag{14}$$

In order to stabilise (14), we choose the intermediate control virtual, x_e, based on DSC as shown in the following equation:

$$x_e = -K_1S_1 \tag{15}$$

where K_1 is a positive design constant.

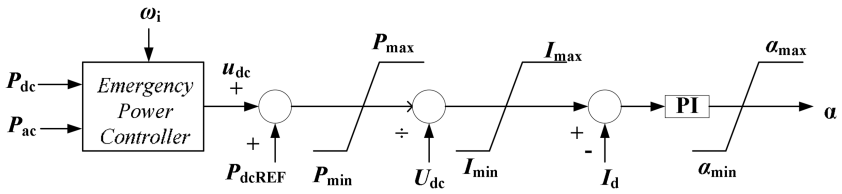

Fig. 3 *Configuration of LCC HVDC emergency power control*

Next we combine adaptive control with DSC to design virtual control rule of LCC HVDC system emergency power controller, which can deal with these parameter uncertainties, we consider the second quadratic function as shown in the following equation:

$$V_2 = \frac{1}{2}S_2^2 + \frac{1}{2\gamma_1}\phi^2 + \frac{1}{2\gamma_2}\chi^2 \tag{16}$$

where $\phi(t) := \theta(t) - \theta^*$, $\chi(t) := \psi(t) - \psi^M$. θ and ψ are the parameters estimate of θ^* and ψ^M, respectively, needed to design-based adaptive control. $\psi^M = \max\{\psi^*, \psi^0\}$, ψ^0 is the initial estimate of ψ^*. $\phi(t)$, $\chi(t)$ are the estimate errors.

Considering (9) and (10), the time derivative of V_2 can be expressed as

$$\begin{aligned}\dot{V}_2 &= S_2\dot{S}_2 + \frac{1}{\gamma_1}\phi\dot{\theta} + \frac{1}{\gamma_2}\chi\dot{\psi} \\ &= S_2(v + \theta^* x_2 + \Delta(t) - \dot{x}_{2d}) + \frac{1}{\gamma_1}\phi\dot{\theta} + \frac{1}{\gamma_2}\chi\dot{\psi}\end{aligned} \tag{17}$$

In order to stabilise (17) and deal with the parameter uncertainty, we design the virtual control rule, v, as shown in the following equation:

$$v = -K_2 S_2 - \theta x_2 - \beta(x, \psi) + \dot{x}_{2d} \tag{18}$$

The specific adaptive control scheme is chosen as

$$\begin{cases} \beta(x, \psi) = \dfrac{S_2\psi^2\omega^2(x)}{S_2\psi\omega(x) + \delta} \\ \dot{\theta}(t) = \gamma_1[S_2 x_2 - \sigma_1(\theta - \theta^0)] \\ \dot{\psi}(t) = \gamma_2[S_2\omega(x) - \sigma_2(\psi - \psi^0)] \\ \omega(x) = \tanh\left(\dfrac{S_2}{\varepsilon}\right) \end{cases} \tag{19}$$

where K_2 is a positive design constant based on DSC, θ and β are the design adaptive control component based on adaptive control using certainty equivalence principle and a variant of the σ-modification, respectively. θ is the parameter estimate of θ^*, β is the control component to handle the uncertain integrated modelling error and integrated external disturbance, ψ is the parameter estimate of ψ^M. δ, ε, γ_1, γ_2, σ_1, σ_2, θ^0, ψ^0 are the positive design parameters and θ^0 can be considered as initial estimates of the unknown θ^*.

Based on the virtual control rule described by (9), the actual LCC HVDC emergency control signal, u_{dc}, can be expressed as

$$\begin{aligned}u_{dc} = &\frac{H_{T,B}T_d(\sum_{i\in A}\dot{P}_{mi} - \dot{P}_{LA} - \dot{P}_{ac})}{H_{T,A} + H_{T,B}} \\ &-\frac{H_{T,A}T_d(\sum_{i\in B}\dot{P}_{mi} - \dot{P}_{LB} + \dot{P}_{ac})}{H_{T,A} + H_{T,B}} \\ &-\frac{2H_{T,A}H_{T,B}T_d v}{H_{T,B} + H_{T,A}} + P_{dc} - P_{dcREF}\end{aligned} \tag{20}$$

where the virtual control rule, v, is calculated as (18).

Owing to the dynamic characteristic of prime mover power input and sum of load and network power loss changes slower than the dynamic characteristic of LCC HVDC system, we set that

$$\dot{P}_{mi} = 0, \quad \dot{P}_{LA} = 0, \quad \dot{P}_{LB} = 0 \tag{21}$$

Furthermore, $\dot{P}_{ac}$ can be got through differential operation achieved by the digital sample system.

The configuration of proposed LCC HVDC emergency power control is shown in Fig. 3.

3.3 Stability analysis

Lemma 1 [24]: For bounded initial conditions $x(t)$, if there exists a $C1$ continuous and positive-definite Lyapunov function $V(t)$, the time derivative of $V(t)$, $\dot{V}(t)$, satisfy that $\dot{V} \le -kV(t) + c$ and k and c are positive constants, $k/c > 0$, then the $x(t)$ uniformly bounded.

Stability Proof: To prove the AC–DC parallel system is stable under the proposed LCC HVDC emergency control strategy, we consider the Lyapunov function of the system as shown in the following equation:

$$V = \frac{1}{2}y_2^2 + \frac{1}{2}V_1^2 + \frac{1}{2}V_2^2 \tag{22}$$

Considering (11), (13) and (15), the time derivative of y_2 can be expressed as

$$\dot{y}_2 = -\frac{y_2}{\tau} + K_1\dot{S}_1 \tag{23}$$

Considering (14), (15), (17), (19) and (23), according to the virtual control rule described by (18) and adaptive control schemes described by (19), we can obtain the time derivative of V as shown in the following equation:

$$\begin{aligned}\dot{V} &= y_2\dot{y}_2 + S_1\dot{S}_1 + \dot{S}_2 S_2\dot{S}_2 + \frac{1}{\gamma_1}\phi\dot{\theta} + \frac{1}{\gamma_2}\chi\dot{\psi} \\ &= -\frac{y_2^2}{\tau} + y_2K_1\dot{S}_1 - K_1S_1^2 + S_1S_2 + S_1y_2 \\ &\quad -k_2S_2^2 + \delta\left[\frac{S_2\psi\omega}{S_2\psi\omega + \delta}\right] + S_2\Delta - S_2\psi^M\omega \\ &\quad -\phi\sigma_1(\theta - \theta^0) - \chi\sigma_1(\psi - \psi^0)\end{aligned} \tag{24}$$

Considering (9), (10), (13) and (15), we can get $\dot{S}_1$ as shown in the following equation:

$$\dot{S}_1 = S_2 + y_2 - K_1S_1 \tag{25}$$

Based on the assumption of DSC, S_1, y_2, S_2 are bounded and $[S_1, y_2, S_2]$ belong to a compact set $A := \{S_1^2 + y_2^2 + S_2^2 \le p\}$, so $\dot{S}_1$ is bounded by a continue function and has a maximum [17, 18]. What's more, K_1 is a positive design parameter, so we can get the inequality as shown in the following equation:

$$|K_1\dot{S}_1| \le M \tag{26}$$

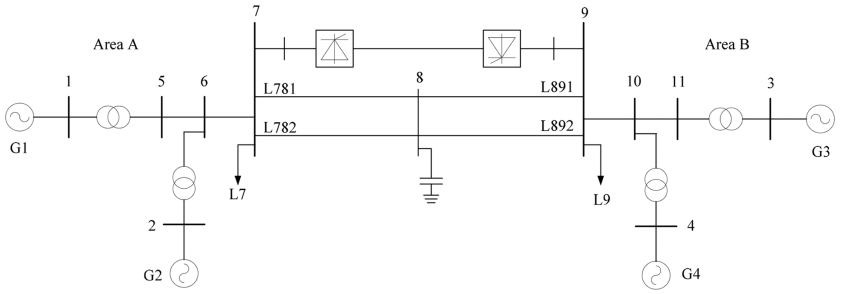

Fig. 4 *Two-area four-generator AC/DC parallel power system*

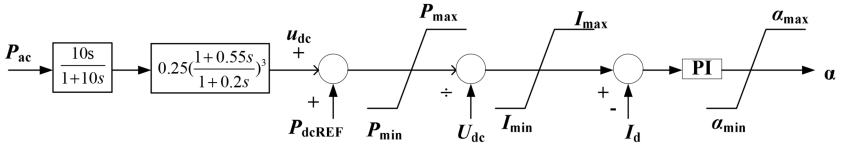

Fig. 5 *Diagram of LCC HVDC emergency controller based on pole placement method*

We adopt the following variable substitution as shown in the following equation:

$$K_1 = K_2 = 2 + \alpha_0, \quad \frac{1}{\tau} = 1 + \frac{M^2}{2\varpi} + \alpha_0 \tag{27}$$

where $\alpha_0 > 0$, $\varpi > 0$

Based on Young's inequality shown in Lemma 3 shown in the Appendix, we can get the inequality as shown in the following equation:

$$|y_2|M \le \frac{M^2 y_2^2}{2\varpi} + \frac{\varpi}{2} \tag{28}$$

Considering (22), (24) and (26)–(28), we can get the inequality about the Lyapunov function as shown in the following equation:

$$\begin{aligned} \dot{V} &\le -\alpha_0 S_1^2 - \alpha_0 S_2^2 - \alpha_0 y_2^2 - \frac{\sigma_1}{2}\phi^2 - \frac{\sigma_2}{2}\chi^2 \\ &\quad + \delta + \frac{\varpi}{2} + \frac{1}{2}\psi^{\mathrm{M}}\varepsilon + \frac{\sigma_1}{2}(\theta^* - \theta)^2 + \frac{\sigma_2}{2}(\psi^M - \psi^0)^2 \\ &\le -CV + \lambda \end{aligned} \tag{29}$$

where

$$C = \min\{2\alpha_0, \sigma_1\gamma_1, \sigma_2\gamma_2\},$$

$$\lambda = \delta + \frac{\varpi}{2} + \frac{1}{2}\psi^{\mathrm{M}}\varepsilon + \frac{\sigma_1}{2}(\theta^* - \theta)^2 + \frac{\sigma_2}{2}(\psi^M - \psi^0)^2$$

According Lemma 1, we can get that $S(t)$, $\theta(t)$, $\psi(t)$ are globally uniformly ultimately bounded, and because the relationship between $S(t)$ and $x(t)$ as shown in (10), we can get that $x(t)$ are globally uniformly ultimately bounded. □

Remark 1: We set that $\rho = \lambda/C$, then Lyapunov function of the system, $V(t)$, satisfies

$$0 \le V(t) \le \rho + (V(0) - \rho)\mathrm{e}^{-ct} \tag{30}$$

If the design parameters K_1, K_2, τ, δ, ε, γ_1, γ_2, σ_1, σ_2, θ^0, ψ^0 are chosen appropriately, then it is possible to make ρ as small as desired, there exists T such that for all $t \ge T$, we can obtain that $|S_i| \le \sqrt{2\rho}$, $i = 1, 2$. Since $x_1 = S_1$, so when $t \ge T$, we can obtain that $|x_1| \le \sqrt{2\rho}$.

It means that when using the control rule described by (18) and adaptive control scheme described by (19), the AC–DC parallel system is stable. Furthermore, the performance of this controller has a direct relationship with the selection of design parameters.

4 Simulation analysis

4.1 Simulation system

The two-area four-generator AC–DC parallel power system shown in Fig. 4 is chosen a test system to illustrate the practical implementation of the proposed emergency power support controller. The parameters and power flow of the test system are given in [5]. The test system model is simulated in the PSCAD/EMTDC. The developed model has the following features:

- LCC HVDC system uses the electromagnetic transient model.
- Constant DC current control is used in the rectifier.
- Constant extinction angle control is used in the inverter.
- Generators use electromagnetic transient model.
- Excitation system uses the static exciter.
- Coordination of the power system stabiliser and the LCC HVDC emergency control strategy is not considered in this paper.

4.2 Performance of the proposed emergency control

The following controller parameters were chosen by means of find-and-error approach with time domain simulations, $K_1 = 20$, $K_2 = 20$, $\tau = 0.0001$, $\delta = 0.001$, $\varepsilon = 0.0005$, $\gamma_1 = 100$, $\gamma_1 = 100$, $\sigma_1 = 0.1$, $\sigma_2 = 0.2$, $\psi^0 = 0.001$; $\theta^0 = 0.001$. The $P_{\max}$ and $P_{\min}$ are $P_{\max} = 1.17$ and $P_{\min} = 0.5$, respectively.

In order to verify the effectiveness of the proposed emergency controller, different faults and different operating points are considered. The results are compared with the LCC HVDC emergency controllers based on (a) pole placement method and (b) backstepping method. The configuration of LCC HVDC emergency controller based on pole placement is shown in Fig. 5 and the parameters of this controller are obtained from [5]. The configuration of the backstepping technique-based LCC HVDC emergency controller is similar to the configuration of the proposed method and the parameters of this controller are obtained from [12].

The following cases are presented:

Case 1: The transmitted power of LCC HVDC system is 201 MW. A three-phase-to-ground fault close to bus 9 occurs on line L892 at 20 s and the fault duration is 0.1 s, the line L892 is tripped at 20.1 s and the LCC HVDC system emergency control is started at 21 s.

Case 2: The transmitted power of LCC HVDC system is 201 MW. A three-phase-to-ground fault close to bus 9 occurs on line L892 at 20 s and the fault duration is 0.2 s, the line L892 is tripped at 20.2 s and the LCC HVDC system emergency control is started at 21 s.

Case 3: The transmitted power of LCC HVDC system is 150.75 MW. A three-phase-to-ground fault close to bus 9 occurs in line L892 at 50 s and the fault duration is 0.2 s, the line L892 is tripped

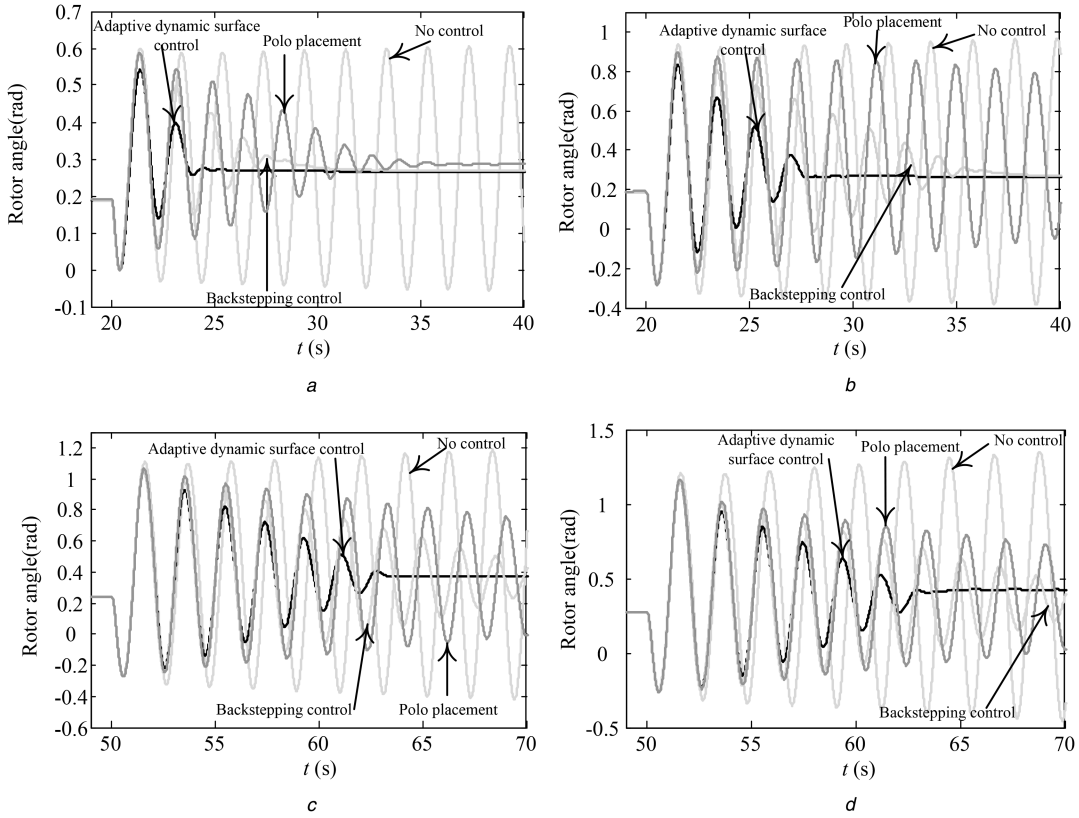

Fig. 6 *The rotor angle of G1*
(a) Case 1, ***(b)*** Case 2, ***(c)*** Case 3, ***(d)*** Case 4

at 50.2 s and the LCC HVDC system emergency control is started at 51 s.

Case 4: The transmitted power of LCC HVDC system is 120.6 MW. A three-phase-to-ground fault close to bus 9 occurs in line L892 at 50 s and the fault duration is 0.2 s, the line L892 is tripped at 50.2 s and the LCC HVDC system emergency control is started at 51 s.

Choose the rotor angle of Generator G3 as the reference, the rotor angle of G1 with respect to G3 with different control schemes in Cases 1–4 is shown in Fig. 6. The dynamics of the power fluctuations on the line L781 in Cases 1–4 are shown in Fig. 7. The dynamics of the power fluctuations of LCC HVDC system with different control schemes are shown in Fig. 8.

From Figs. 6–8, we can see that the system is unstable after the disturbance without emergency controller. When the proposed LCC HVDC emergency control strategy and the other two LCC HVDC emergency control strategies are applied to the test power system in Case 1, the rotor angle of generator G1 and power flow of interconnected AC line under the control of the proposed LCC HVDC emergency control strategy have better damping and the system become stable quicker than the other two methods.

Further, the LCC HVDC emergency control strategy based on pole placement is a linear method. Therefore, the performance of this control strategy depends on how close the operating state is to the equilibrium point. When a fault is applied for a long period, the system state is further away from the equilibrium point and the non-linear behaviour comes into play. The results of Figs. 6–8 show that under such conditions, the proposed non-linear controller performs better than the pole placement controller. Therefore, the effectiveness and feasibility of the proposed HVDC emergency control strategy have been verified.

4.3 Impact of time delay

It is well known that there exists time delay in the WAMS. In order to verify that the proposed control strategy is robust to the time delay, two time delay cases are considered: (i) angular velocity of generators and power signals of AC and DC lines is delayed by 50 ms, and (ii) angular velocities of generators and power signals of AC and DC lines are delayed by 30 and 50 ms, respectively. The fault type is same as the Case 1 in Section 2.

The rotor angle of G1 with respect to G3 with different time delays is shown in Fig. 9*a*. The dynamics of the power fluctuations on the line L781 and LCC HVDC system with different time delays are shown in Figs. 9*b* and *c*, respectively.

From Fig. 9, it is evident that the proposed controller is stable in the presence of time delay. Therefore, the robustness of the proposed control strategy to time delay has been verified.

5 Conclusions

In this paper, an LCC HVDC wide-area emergency power control strategy is designed based on the DSC and adaptive control schemes. The purpose of the design is to use the global signals of the AC–DC parallel system and make a continuous and simple control rule which can deal with the parameter uncertainty, unknown modelling error and external disturbance. Simulation results verify the effectiveness and correctness of the proposed LCC HVDC wide-area emergency power control strategy and the robustness of proposed LCC HVDC emergency power control strategy to the time delay. It also shows that the proposed LCC HVDC emergency power control strategy is adaptive to different fault types and different operating points and has better performance than the LCC HVDC emergency power control strategy based on the backstepping technique and pole placement technique.

What's more, the performance of the systems under the coordinated control strategy of the PSS and LCC HVDC based on DSC strategy and adaptive control schemes should be better.

6 Acknowledgments

This work was supported by the National Natural Science Foundation of China (51277068), and supported by the Program for New Century Excellent Talents in University (NCET-12-0846), partially supported by '111' Project (B08013) of China and the 863 Program (2015AA050101).

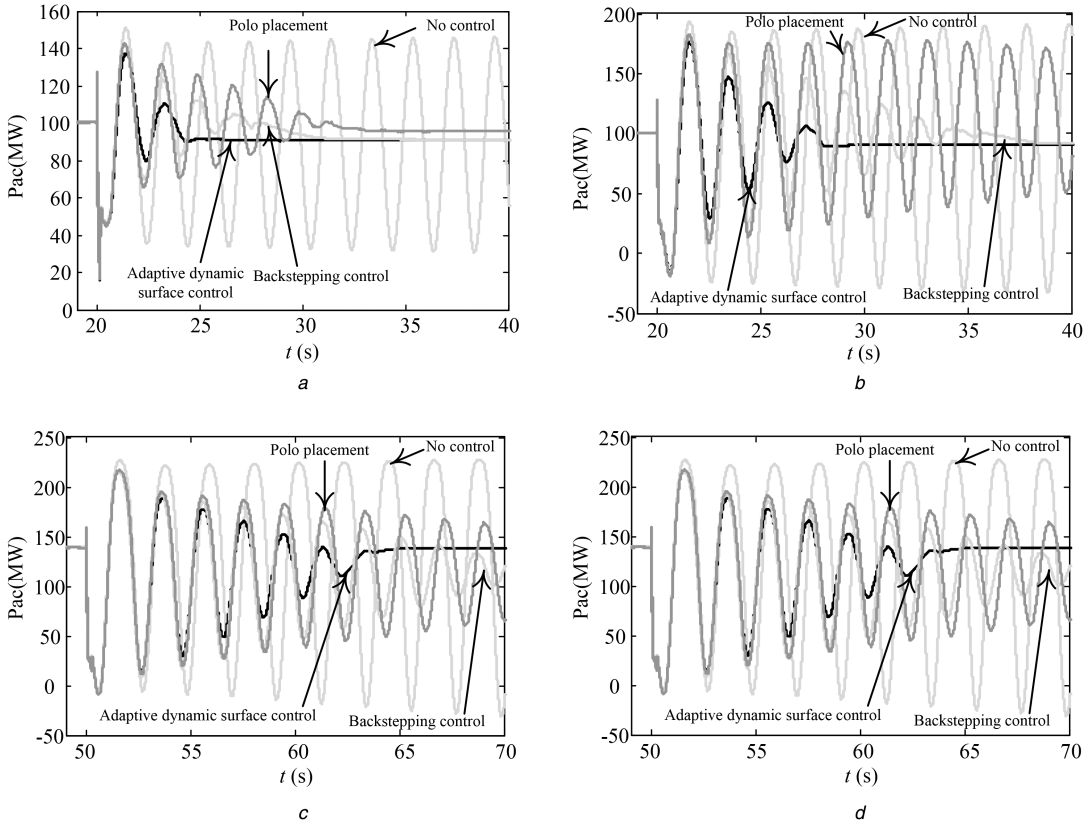

Fig. 7 *The active power of line L781*
(a) Case 1, ***(b)*** Case 2, ***(c)*** Case 3, ***(d)*** Case 4

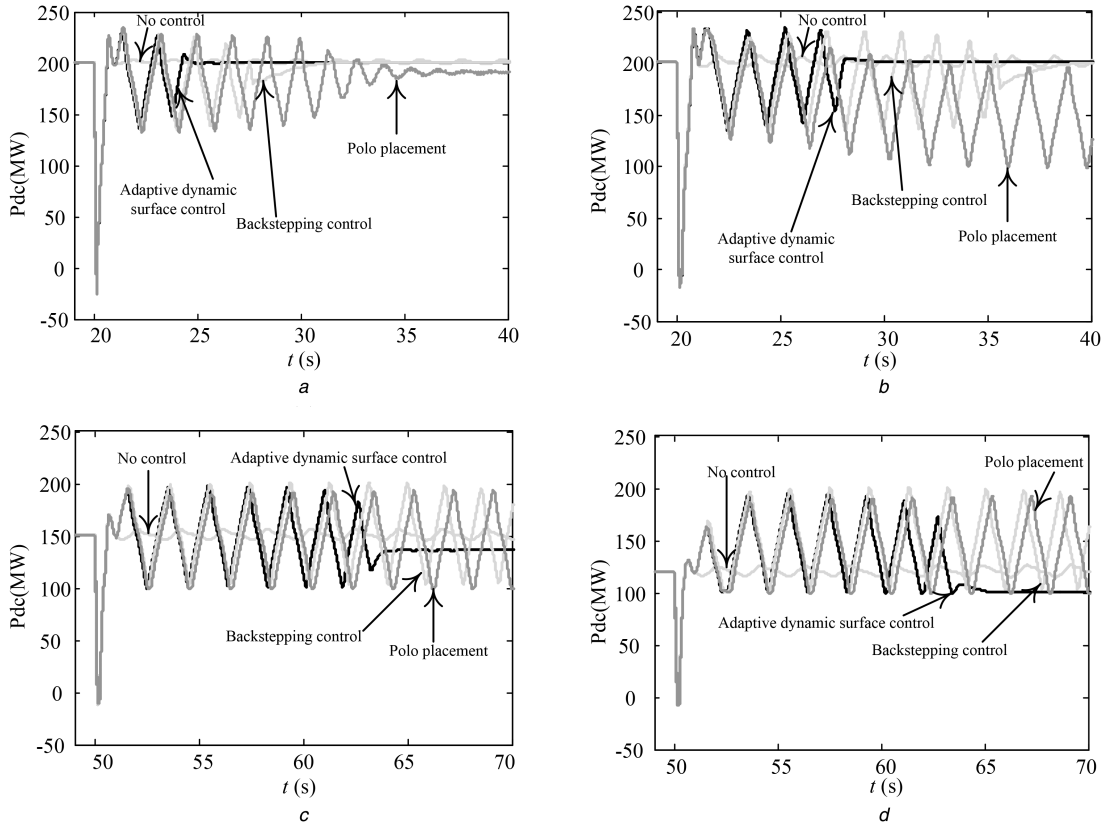

Fig. 8 *The active power of LCC HVDC system*
(a) Case 1, ***(b)*** Case 2, ***(c)*** Case 3, ***(d)*** Case 4

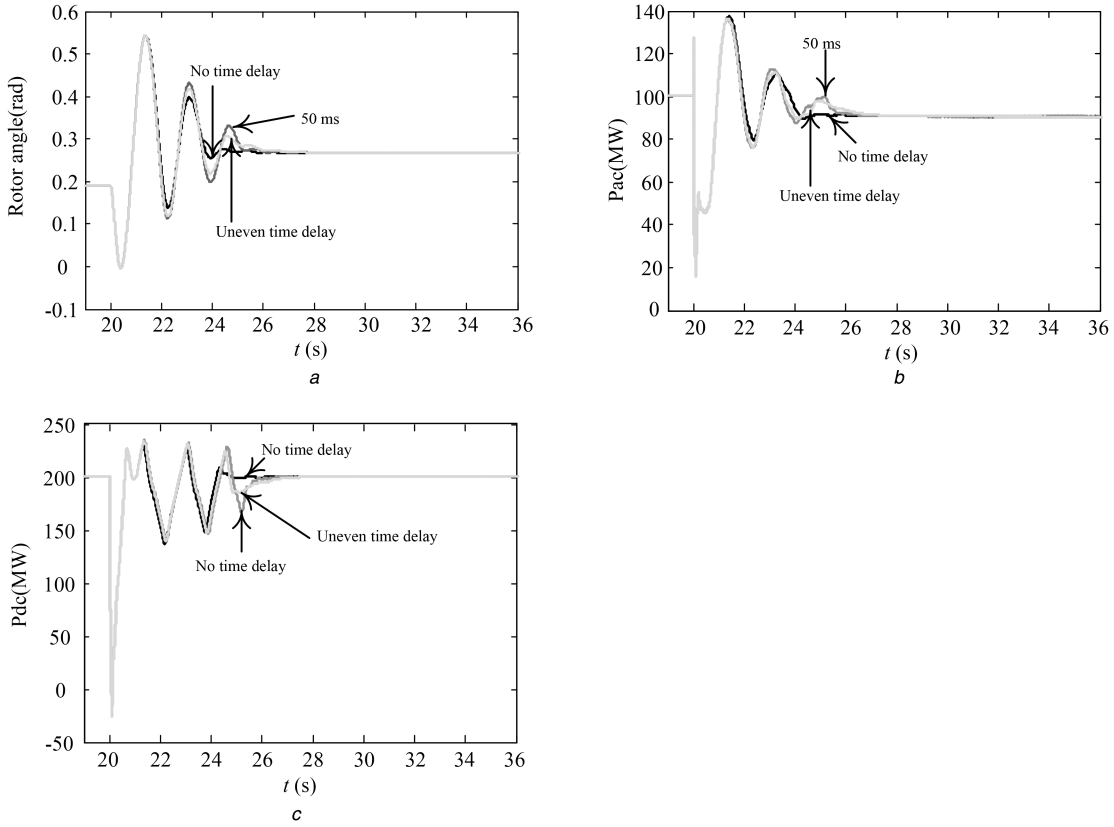

Fig. 9 *System responses with different time delay*

(a) The rotor angle of G1, ***(b)*** The active power of L781, ***(c)*** The active power of LCC HVDC system

7 References

[1] Qin, X., Zeng, P., Zhou, Q., *et al.*: 'Study on the development and reliability of HVDC transmission systems in China'. 2016 IEEE Int. Conf. Power System Technology, Wollongong, 2016, pp. 1–6

[2] Bilodeau, H., Babaei, S., Bisewski, B., *et al.*: 'Making old new again: HVdc and FACTS in the northeastern United States and Canada', *IEEE Power Energy Mag.*, 2016, **14**, (2), pp. 42–56

[3] Bing, L., Jian, S., Shangmao, H., *et al.*: 'New research progress of HVDC transmission technology in China Southern Power Grid Corporation'. IEEE Int. Conf. High Voltage Engineering and Application, Chengdu, 2016, pp. 1–5

[4] Liu, C., Wei, F., Chen, Z., *et al.*: 'Magnitude adaptive emergency power support control technology', *Autom. Electr. Power Syst.*, 2013, **37**, (21), pp. 123–128

[5] Kundur, P.: '*Power system stability and control*' (McGraw-Hill Inc., 1994), pp. 1151–1160

[6] Wenqiang, Z., Yongping, W., Baoli, C., *et al.*: 'Study on frequency control strategy for ORMOC-NAGA HVDC project in Philippines'. 2016 IEEE PES Transmission & Distribution Conf. and Exposition-Latin America, Morelia, 2016, pp. 1–6

[7] Tesfay, T., Le Boudec, J.Y.: 'Experimental comparison of multicast authentication for wide area monitoring systems', *IEEE Trans. Smart Grid*, 2017, **PP**, (99), pp. 1–10

[8] Tokel, H.A., Alirezaei, G., Baig, S., *et al.*: 'An optimization framework for planning of WAMS with a heterogeneous communication network'. IEEE Int. Conf. Smart Grid Communications, Sydney, 2016, pp. 521–526

[9] Ren, B., Zhong, Q.C., Dai, J.: 'Asymptotic reference tracking and disturbance rejection of UDE-based robust control', *IEEE Trans. Ind. Electron.*, 2017, **64**, (4), pp. 3166–3176

[10] Dong, J., Zhang, G.: 'Identification and robust control of the nonlinear photoelectrothermal dynamics of LED systems', *IEEE Trans. Ind. Electron.*, 2017, **64**, (3), pp. 2215–2225

[11] Lin, S., Cai, Y., Yang, B., *et al.*: 'Electrical line-shafting control for motor speed synchronisation using sliding mode controller and disturbance observer', *IET Control Theory Applic.*, 2017, **11**, (2), pp. 205–212

[12] Rajendran, S., Jena, D.: 'Backstepping sliding mode control of a variable speed wind turbine for power optimization', *J. Modern Power Syst. Clean Energy*, 2015, **3**, (3), pp. 402–410

[13] Zhao, Y., Lu, C., Li, P., *et al.*: 'Applications of wide-area adaptive HVDC and generator damping control in Chinese power grids'. IEEE Power and Energy Society General Meeting, Boston, 2016, pp. 1–5

[14] Zhu, H., Zhou, L., Cai, Z., *et al.*: 'Wide area measuring system signals based nonlinear robust adaptive DC power modulation controller in AC/DC interconnected power system', *Autom. Electr. Power Syst.*, 2006, **30**, (7), pp. 21–26

[15] Roberson, D., O'Brien, J.F.: 'Coupling analysis & preliminary MIMO control design for wide-area damping using HVDC'. North American Power Symp., Denver, 2016, pp. 1–6

[16] Sankeswari, S., Chile, R.: 'Sliding mode control for performance improvement of linear systems'. 2016 Int. Conf. Emerging Technological Trends, Kollam, 2016, pp. 1–7

[17] Tchenderli-Braham, S.A., Khebbache, H., Hamerlain, F., *et al.*: 'Dynamic surface control-based stabilization of an nth chained systems with application to a car-like robot'. IEEE/RSJ Int. Conf. Intelligent Robots and Systems, Daejeon, 2016, pp. 5379–5384

[18] Wang, C., Wu, Y., Yu, J.: 'Barrier Lyapunov functions-based dynamic surface control for pure-feedback systems with full state constraints', *IET Control Theory Appl.*, 2017, **11**, (4), pp. 524–530

[19] Zhang, Z., Duan, G., Hou, M.: 'Robust adaptive dynamic surface control of uncertain non-linear systems with output constraints', *IET Control Theory Applic.*, 2017, **11**, (1), pp. 110–121

[20] Yu, J., Ma, Y., Yu, H., *et al.*: 'Adaptive fuzzy dynamic surface control for induction motors with iron losses in electric vehicle drive systems via backstepping', *Inf. Sci.*, 2017, **376**, pp. 172–189

[21] Li, S., Liang, X., Fei, J.: 'Dynamic surface adaptive fuzzy control of three-phase active power filter', *IEEE Access*, 2016, **4**, pp. 9451–9458

[22] Zhou, C., Zhou, D., Huang, B.: 'Robust adaptive dynamic surface attitude control of flexible spacecraft'. 54th Annual Conf. the Society of Instrument and Control Engineers of Japan, Hangzhou, 2015, pp. 510–517

[23] Xu, B.: 'Disturbance observer-based dynamic surface control of transport aircraft with continuous heavy cargo airdrop', *IEEE Trans. Syst. Man Cybern., Syst.*, 2017, **47**, (1), pp. 161–170

[24] Zhou, M.C., Jiang, C.: 'Robust tracking control of uncertain MIMO nonlinear systems with application to UAVs', *IEEE/CAA J. Autom. Sinica*, 2015, **2**, (1), pp. 25–32

[25] Yu, J., Shi, P., Dong, W., *et al.*: 'Neural network-based adaptive dynamic surface control for permanent magnet synchronous motors', *IEEE Trans. Neural Netw. Learn. Syst.*, 2015, **26**, (3), pp. 640–645

[26] Teng, T., Yang, C., Xu, B.: 'Neural network based global adaptive dynamic surface tracking control for robot manipulators'. Int. Conf. Advanced Robotics and Mechatronics, Macau, 2016, pp. 20–25

[27] Lei, D., Wang, T., Cao, D., *et al.*: 'Adaptive dynamic surface control of MEMS gyroscope sensor using fuzzy compensator', *IEEE Access*, 2016, **4**, pp. 4148–4154

[28] Wen, S., Chen, M.Z.Q.: 'Fuzzy control for uncertain vehicle active suspension systems via dynamic sliding-mode approach', *IEEE Trans. Syst. Man Cybern., Syst.*, 2017, **47**, (1), pp. 24–32

[29] Tang, G., Xu, Z., Dong, H., *et al.*: 'Sliding mode robust control based active-power modulation of multi-terminal HVDC transmissions', *IEEE Trans. Power Syst.*, 2016, **31**, (2), pp. 1614–1623

[30] Xu, S., Yang, Y., Yi, J.: 'A polytopic system theory approach to wide-area decentralized coordinated control of HVDC system'. IEEE Int. Conf. Cyber Technology in Automation, Control, and Intelligent Systems, Shenyang, 2015, pp. 1605–1610

8 Appendix

Lemma 2 [24]: For $\forall\beta > 0$, $\forall u \in R$, the following inequality always holds:

$$0 \le |u| - u\tanh\left(\frac{u}{\beta}\right) \le K\beta$$

where K is a constant that satisfies $K = e^{-(K-1)}$; e.g. $K = 0.2785$.

Lemma 3: Young's inequality

$$\left(\frac{Z^2\rho^2}{2\mu}\right) + \left(\frac{\mu}{2}\right) \ge |Z|\rho$$

8.1 Virtual control variable of the system v

Substitute (9) with (4), (6) and (8), the state space of AC–DC parallel system can be expressed as

$$\begin{aligned}
\dot{x}_1 &= x_2 \\
\dot{x}_2 &= \frac{\sum_{i\in A}\dot{P}_{\mathrm{mi}} - \dot{P}_{\mathrm{LA}} - \dot{P}_{\mathrm{ac}} - \dot{P}_{\mathrm{dc}}}{2H_{T,A}} - \frac{\sum_{i\in B}\dot{P}_{\mathrm{mi}} - \dot{P}_{\mathrm{LB}} + \dot{P}_{\mathrm{ac}} + \dot{P}_{\mathrm{d}}}{2H_{T,B}} \\
&= \frac{\sum_{i\in A}\dot{P}_{\mathrm{mi}} - \dot{P}_{\mathrm{LA}} - \dot{P}_{\mathrm{ac}}}{2H_{T,A}} - \frac{\sum_{i\in B}\dot{P}_{\mathrm{mi}} - \dot{P}_{\mathrm{LB}} + \dot{P}_{\mathrm{ac}}}{2H_{T,B}} \\
&\quad - \frac{(H_{T,B}+H_{T,A})}{2H_{T,A}H_{T,B}}\left[\frac{1}{T_d}(-P_{\mathrm{dc}} + P_{\mathrm{deREF}} + u_{\mathrm{dc}})\right] \\
&\quad + \underset{\mathrm{COI}}{\tilde{D}}(\dot{\omega}_{\mathrm{COI},A} - \dot{\omega}_{\mathrm{COI},B}) - \frac{(H_{T,B}+H_{T,A})}{2H_{T,A}H_{T,B}}e_D + \dot{e}_R + \dot{e}_G
\end{aligned}$$

Using the v represents the virtual control variable of the system, θ^* represents the uncertain COI-based equivalent damping factor $\underset{\mathrm{COI}}{\tilde{D}}$, $\Delta(t)$ is used to represent the uncertain integrated modelling error and integrated external disturbance. Then the state space of AC–DC parallel system can be shown as the following equation:

$$\begin{cases} \dot{x}_1 = x_2 \\ \dot{x}_2 = v + \theta^* x_2 + \Delta(t) \end{cases}$$

where

$$\begin{aligned}
v &= \frac{\sum_{i\in A}\dot{P}_{\mathrm{mi}} - \dot{P}_{\mathrm{LA}} - \dot{P}_{\mathrm{ac}}}{2H_{T,A}} - \frac{\sum_i \dot{P}_{\mathrm{mi}} - \dot{P}_{\mathrm{LB}} + \dot{P}_{\mathrm{ac}}}{2H_{T,B}} \\
&\quad - \frac{(H_{T,B}+H_{T,A})}{2H_{T,A}H_{T,B}}\left[\frac{1}{T_d}(-P_{\mathrm{dc}} + P_{\mathrm{deREF}} + u_{\mathrm{dc}})\right], \\
\theta^* &= \underset{\mathrm{COI}}{\tilde{D}}, \\
\Delta(t) &= -\frac{(H_{T,B}+H_{T,A})}{2H_{T,A}H_{T,B}}e_D + \dot{e}_R + \dot{e}_G .
\end{aligned}$$

8.2 Time derivative of S1

Considering (9), (10) and (13), the time derivative of S_1 can be expressed as

$$\begin{aligned}
\dot{S}_1 &= \dot{x}_1 = x_2 = S_2 + x_{2d} \\
&= S_2 + y_2 + x_e
\end{aligned}$$

8.3 Time derivative of y_2

Considering (11), (13) and (15), the time derivative of y_2 can be expressed as

$$\dot{y}_2 = \dot{x}_{2d} - \dot{x}_e = \frac{x_e - x_{2d}}{\tau} - \dot{x}_e = -\frac{y_2}{\tau} + K_1\dot{S}_1$$

8.4 Time derivative of V

Considering (14), (15), (17)–(19) and (23), the time derivative of V can be expressed as

$$\begin{aligned}
\dot{V} &= y_2\dot{y}_2 + S_1\dot{S}_1 + S_2\dot{S}_2 + \frac{1}{\gamma_1}\phi\dot{\theta} + \frac{1}{\gamma_2}\chi\dot{\psi} \\
&= -\frac{y_2^2}{\tau} + y_2K_1\dot{S}_1 - k_1S_1^2 + S_1S_2 + S_1y_2 \\
&\quad + S_2[-k_2S_2 - (\theta-\theta^*)x_2 - (\beta-\Delta)] \\
&\quad + \frac{1}{\gamma_1}\phi\{\gamma_1[S_2x_2 - \sigma_1(\theta-\theta^0)]\} + \frac{1}{\gamma_2}\chi\{\gamma_2[S_2\omega - \sigma_1(\psi-\psi^0)]\} \\
&= -\frac{y_2^2}{\tau} + y_2K_1\dot{S}_1 - k_1S_1^2 + S_1S_2 + S_1y_2 - k_2S_2^2 - S_2\beta + S_2\Delta \\
&\quad - \phi\sigma_1(\theta-\theta^0) + S_2\chi\omega - \chi\sigma_1(\psi-\psi^0) \\
&= -\frac{y_2^2}{\tau} + y_2K_1\dot{S}_1 - k_1S_1^2 + S_1S_2 + S_1y_2 - k_2S_2^2 - \frac{S_2^2\psi^2\omega^2}{S_2\psi\omega+\delta} \\
&\quad + S_2\Delta + S_2\psi\omega - S_2\psi^M\omega - \phi\sigma_1(\theta-\theta^0) - \chi\sigma_1(\psi-\psi^0) \\
&= -\frac{y_2^2}{\tau} + y_2K_1\dot{S}_1 - k_1S_1^2 + S_1S_2 + S_1y_2 - k_2S_2^2 + \delta\left[\frac{S_2\psi\omega}{S_2\psi\omega+\delta}\right] \\
&\quad + S_2\Delta - S_2\psi^M\omega - \phi\sigma_1(\theta-\theta^0) - \chi\sigma_1(\psi-\psi^0)
\end{aligned}$$

8.5 Inequality about the time derivative of V

For $\forall S_2 \in R, \forall t \in R^+$, it can be shown that $S_2\psi\omega > 0$, so we can get the inequality as shown below:

$$\delta\left[\frac{S_2\psi\omega}{S_2\psi\omega+\delta}\right] < \delta$$

Based on Lemma 2, we can get the inequality as shown below:

$$\begin{aligned}
S_2\Delta - S_2\psi^M\omega &\le \psi^M(|S_2| - S_2\omega) \\
&= \psi^M\left[|S_2| - S_2\tanh\left(\frac{S_2}{\varepsilon}\right)\right] \le \frac{1}{2}\psi^{\mathrm{M}}\varepsilon
\end{aligned}$$

By completing the square, we can get the equality as shown below:

$$\begin{cases}
-\sigma_1\phi(\theta-\theta^0) = -\frac{\sigma_1}{2}\phi^2 - \frac{\sigma_1}{2}(\theta-\theta^0)^2 + \frac{\sigma_1}{2}(\theta^*-\theta^0)^2 \\
-\sigma_2\chi(\psi-\psi^0) = -\frac{\sigma_2}{2}\chi^2 - \frac{\sigma_2}{2}(\psi-\psi^0)^2 + \frac{\sigma_2}{2}(\psi^M-\psi^0)^2
\end{cases}$$

Considering (24), (26) and the equality and inequality as shown above, we can get the inequality about the time derivative of Lyapunov function as shown below:

$$\begin{aligned}
\dot{V} &\le -\left(K_1S_1^2 + K_2S_2^2 + \frac{\sigma_1}{2}\phi^2 + \frac{\sigma_2}{2}\chi^2 + \frac{y_2^2}{\tau}\right) \\
&\quad + S_1(S_2+y_2) + \delta + \frac{1}{2}\psi^M\varepsilon + \frac{\sigma_1}{2}(\theta^*-\theta)^2 \\
&\quad + \frac{\sigma_2}{2}(\psi^M-\psi^0)^2 + |y_2|M
\end{aligned}$$

Considering (22), (27) and (28), the inequality about the time derivative of Lyapunov function can be expressed as

$$
\begin{aligned}
\dot{V} \le & -(2+\alpha_0)S_1^2 - (2+\alpha_0)S_2^2 - \frac{\sigma_1}{2}\phi^2 - \frac{\sigma_2}{2}\chi^2 \\
& -\left(1+\frac{M^2}{2\varpi}+\alpha_0\right)y_2^2 + S_1(S_2+y_2) + \delta + \frac{1}{2}\psi^{\mathrm{M}}\varepsilon \\
& +\frac{\sigma_1}{2}(\theta^*-\theta)^2 + \frac{\sigma_2}{2}(\psi^M-\psi^0)^2 + \frac{M^2y_2^2}{2\varpi} + \frac{\varpi}{2} \\
= & -\alpha_0 S_1^2 - \alpha_0 S_2^2 - \alpha_0 y_2^2 - \frac{\sigma_1}{2}\phi^2 - \frac{\sigma_2}{2}\chi^2 \\
& +\delta + \frac{\varpi}{2} + \frac{1}{2}\psi^{\mathrm{M}}\varepsilon + \frac{\sigma_1}{2}(\theta^*-\theta)^2 + \frac{\sigma_2}{2}(\psi^M-\psi^0)^2 \\
& -2S_1^2 - 2S_2^2 - y_2^2 + S_1S_2 + S_1y_2 \\
\le & -\alpha_0 S_1^2 - \alpha_0 S_2^2 - \alpha_0 y_2^2 - \frac{\sigma_1}{2}\phi^2 - \frac{\sigma_2}{2}\chi^2 \\
& +\delta + \frac{\varpi}{2} + \frac{1}{2}\psi^{\mathrm{M}}\varepsilon + \frac{\sigma_1}{2}(\theta^*-\theta)^2 + \frac{\sigma_2}{2}(\psi^M-\psi^0)^2 \\
\le & -CV + \lambda
\end{aligned}
$$

where

$$
\begin{aligned}
C = & \ \min\{2\alpha_0, \sigma_1\gamma_1, \sigma_2\gamma_2\}, \\
\lambda = & \ \delta + \frac{\varpi}{2} + \frac{1}{2}\psi^{\mathrm{M}}\varepsilon + \frac{\sigma_1}{2}(\theta^*-\theta)^2 + \frac{\sigma_2}{2}(\psi^M-\psi^0)^2
\end{aligned}
$$